1 Abstract

1. Body size is one of the most important traits governing individual-level demographic rates and modulating population-level processes. Multiple size-dependent demographic rates can simultaneously change population structure, so distinguishing their individual contributions to overall population dynamics remains a challenge.

2. Disentangling size-dependent harvest rates from other demographic rates is critical for assessing the impact of removal on populations of invasive species. Inference about invasive populations can be difficult, however, as observations are often collected opportunistically as part of removal programs, rather than experimentally designed. Yet accurate inference is essential for understanding the feasibility of population suppression and optimizing management decisions.

3. We develop an integrated integral projection model (IPM^2) that leverages the strengths of the integrated population model and integral projection model to enable inference about complex, size-structured demographic rates from imperfect observations. We apply the IPM^2 in the context of invasive European green crab (*Carcinus maenas*), a species for which individual body size strongly regulates both the observation-generating process and latent, population dynamics.

4. The IPM^2 facilitates the distinct estimation of green crab size-structured harvest and natural mortality rates, parameters for which no explicit data is collected and that are unidentifiable in component datasets of the integrated population model. The model represents how the green crab population changes over time, providing the first estimates of size-structured abundance of this high priority species.

5. By forecasting the stable size distribution and equilibrium population size under varying removal efforts, we demonstrate that extremely high levels of removal effort can reduce the equilibrium green crab population size. Yet these high mortality rates also shift the stable size distribution and increase the equilibrium abundance of smaller crabs, since size-selective removal alters intra-specific interactions. The ecological outcome of this shift in size-structure will be variable, as green crab size modulates only some of its interactions with other species. These results highlight the value of the IPM^2 framework for inferring complex population dynamics with information needs that outpace information in individual observational datasets, providing a path forward for accurate assessment of conservation programs.

Key words: integrated population model, integral projection model, state-space framework, invasive species, European green crab, size structure

2 Introduction

Assessing the efficacy of invasive species management interventions requires understanding if and how removal actions change population abundance and dynamics. However, effective population suppression can be challenging to differentiate from natural biological variation, reflecting the perennial challenge of distinguishing harvest and natural mortality (Aanes et al., 2007). Often variability in harvest mortality is confounded with variability in natural mortality (Lewy & Nielsen, 2003), yet separating these fluctuations is crucial for understanding population processes and designing effective management strategies (Walters & Martell, 2004). Invasive species removal program success is highly variable (Prior et al., 2018), so reliably quantifying harvest rates is essential for evaluating intervention success and efficiently allocating limited management resources (Green & Grosholz, 2021).

This challenge of disentangling sources of mortality is amplified for species with complex, size-structured demography. Body size can determine the strength of ecological interactions an individual experiences and can influence its key life-history processes like growth and mortality (De Roos et al., 2003). The ontogenetic scaling of ecological performance with body size can ultimately drive patterns at the population level (Werner, 1994). Population dynamics can be shaped by competitive and predatory (cannibalistic) intra-specific interactions between different size cohorts (Claessen et al., 2004), predator-prey size-dependent functional responses (Aljetlawi et al., 2004), variable reproductive capacity across size (Hixon et al., 2014), and size-selective rates of harvest (Tu et al., 2018). Since these size-structured rates and interactions simultaneously modulate population dynamics, unraveling their individual contributions can be difficult and require substantial amounts of well-structured data.

This poses a particular challenge in the context of monitoring invasive species populations, where ecologists are often limited to removal sampling data (Udell et al., 2022), which are typically collected opportunistically as part of removal programs, rather than experimentally designed (Crall et al., 2010; Rogosch & Olden, 2021; Tiberti et al., 2021). Consequently, these data fail to meet the strict assumptions of models commonly used to estimate abundance with animals removed successively from multiple sites for closed populations (Dorazio et al., 2005). These removal observations are often not collected systematically across time and space and can be associated with large measurement error that can mask biological signals (Auger-Méthé et al., 2016; Katsanevakis et al., 2012; Sibert et al., 2003).

Despite the unique statistical inference challenges associated with invasive species removal data, the costs of under- or over-estimating removal harvest rates can be high. Ineffective invasive population suppression plans waste human and economic resources and can degrade the confidence of people and stakeholders involved in removal (Tiberti et al., 2021). As invasive species management becomes more ambitious in scope

and scale, population control can be controversial, stimulating conflicts among people and debates about achievability and efficiency (Crowley et al., 2017). These undesirable social outcomes underscore the need for rigorous assessments of the effectiveness of control programs.

Combining existing classes of models can be useful for distinguishing process from observation dynamics, facilitating parameter identifiability, and enabling inference about complex, size-structured demographic rates from imperfect observations. Two attractive frameworks are integral projection models and integrated population models. On the one hand, an integral projection model can be used to make population projections based on vital rates that vary continuously as a function of body size (Merow et al., 2014; Rees et al., 2014). In contrast to matrix population models that can produce artifacts from coarse, arbitrary size class divisions, the integral projection model enables modeling of biological realism by using smooth relationships between individual size and demographic performance (Ellner & Rees, 2006). Formulated in a state-space framework, the integral projection model can be used to model natural variation in ecological processes separately from observation error (Auger-Méthé et al., 2021; White et al., 2016).

On the other hand, integrated population models can resolve parameter identifiability issues in scenarios when information requirements of these complex models exceed information available in a single, limited dataset (Besbeas et al., 2002). By jointly analyzing multiple survey and demographic datasets in an integrated framework, integrated population models increase the precision of parameter estimates and facilitate estimation of "additional" parameters that would otherwise not be identifiable (Abadi et al., 2010; Riecke et al., 2019). Coupling an integrated population model and an integral projection model into an integrated integral projection model (IPM^2) offers a fruitful synergy for understanding complex biological dynamics. While the integral projection model provides a biologically-realistic mathematical representation of size-structured dynamics, the integrated population model can make inference possible via the combined information from multiple datasets. Importantly, the IPM^2 can be used to understand how the relationship between individual size and demographic performance can play a role in population-level processes (Plard et al., 2019).

An IPM^2 will be useful for understanding population dynamics and removal effectiveness of invasive European green crab (*Carcinus maenas*). Listed as one of the world's 100 worst invaders (Lowe et al., 2000), the green crab has multiple documented modes of impact. The green crab is an ecosystem engineer; through its foraging activity, the green crab physically alters eelgrass habitat and reduces the density of this important coastal habitat-forming plant species (Garbary et al., 2014; Howard et al., 2019). The green crab also predates upon and outcompetes other shellfish, including commercially-valuable bivalves like soft-shell clams and manila clams (Fisher et al., 2024; Grosholz et al., 2000). This damage is costly, as potential future shellfish harvest losses due to green crab predation on the U.S. West Coast are forecasted to exceed $45 million per year (Grosholz et al., 2011).

Despite these impacts, the effectiveness of removal is not well characterized, as the crab's population dynamics are highly non-linear and are regulated by complex, size-structured demography. Adult crabs exert direct control of recruitment, largely through strong negative adult-juvenile interactions like cannibalism (Grosholz et al., 2021; Romano & Zeng, 2017). Competition with native crabs is also size-structured, with larger crabs maintaining a competitive advantage for space and resources (Jensen et al., 2007; McDonald et al., 2001). Importantly, these individual, size-structured interactions modulate population-level processes; a field experiment in California, USA found a 30-fold, single-year increase in total green crab abundance in response to a removal program that selected for large adults (Grosholz et al., 2021). This high level of juvenile survival associated with low adult abundance, often referred to as overcompensation or the "hydra effect", underscores the importance of quantifying size-structured population response to removal (Abrams, 2009). The green crab observation process is also size-selective, further complicating distinction between simultaneous size-structured processes. Baited traps used for removal do not catch all individuals with equal probability across size classes, with the larval stage and smaller green crab size classes completely unobserved (Jørgensen et al., 2009). Additionally, the observability of the population changes within a trapping season (April - October), as juvenile individuals that have settled from their larval stage in the spring grow into size classes capable of being caught in traps by the fall. Quantifying the relationship between removal effort and size-structured removal rates will be necessary for assessing the feasibility and impact of removal, understanding long-term dynamics, and optimizing management actions and decisions for this high priority species.

Here we develop an integrated integral projection model (IPM^2) to quantify size-structured harvest rates of invasive European green crab. As part of a state-space framework, process dynamics are described using an integral projection model, where the population structure changes over time through seasonal growth, natural mortality, and removal, and observations are generated through the use of multiple size-selective removal methods (Figure 1). Combining multiple datasets in an integrated framework allows for distinct inference about size-structured harvest and natural mortality rates, both of which are "additional parameters" for which no explicit data is collected. Three datasets contribute to different aspects of the model, with size-at-age data informing seasonal growth rates, mark-recapture data primarily informing natural mortality and trap capture rates, and a multi-year time series dataset merging all components and informing latent and observation processes across multiple years (Figure 2). The IPM^2 facilitates prediction of the stable size distribution and equilibrium abundance under different removal strategies, providing a framework for accurate assessment of the effectiveness of invasive species control programs.

3 Methods and materials

3.1 Study system

While the European green crab (*Carcinus maenas*) has successfully colonized all continents except Antarctica (Yamada, 2001), our analysis focuses on the dynamics of green crab found in the Northeast Pacific along the west coast of North America where the crab's range has been expanding over the last few decades. The first introduced green crab population in the Northeast Pacific was established in San Francisco Bay in the early 1990's. The crab's range has since expanded northward through larval transport in the Davidson Current (Yamada et al., 2021); the green crab expanded into Oregon and Washington coastal estuaries in 1998 and into the Salish Sea in 2016 and 2017.

The European green crab is a resilient marine invader, able to withstand a wide range of environmental conditions and rapidly develop cold tolerance adaptations (Tepolt & Palumbi, 2020). Additionally, the green crab can recolonize quickly after removal, largely due to a mismatch in spatial scale between local removal programs and the crab's wide-ranging dispersal and population processes (Keller et al., 2025). While adult crabs occupy sheltered bays and estuaries, the crab disperses during a larval phase in open marine waters that facilitates recolonization of suppressed populations in neighboring habitats (Yamada et al., 2021). Due to this spatial mismatch and rapid rate of recolonization, some population control measures have had limited utility in sustained suppression over the longer term (Duncombe, 2015; Tummon Flynn et al., 2024).

3.2 Demographic data

Population-level inference is focused on size-structured green crab abundance at Drayton Harbor in Washington, USA in the Salish Sea (Appendix 1.1, Figure A1.1). The primary dataset (D1) comprises a time series of counts of removed crabs collected in April - October from 2020-2023 and is structured by body size (Figure 1B). Multiple trap types (Fukui, Minnow, and Shrimp) with different size-selective removal rates were used (Figure 1B), and traps were baited and left to "soak" in intertidal and subtidal habitat for 24-48 hours. As Drayton Harbor is a protected bay, nearly enclosed by a land spit, we assume a closed population for adults and no movement of non-larval crabs in and out of the study site.

Inference was supplemented by two additional datasets, size-at-age data (D2) and mark-recapture data (D3). Size-at-age data (D2) were collected from crab removal observations associated with range expansions in northeastern Pacific estuaries documented by Yamada et al. 2021. Since the colonizing cohorts of crabs following expansion events were relatively easy to identify as they age over time, Yamada et al. 2021 assigned a year class to captured crabs based on the location of collection, assumed expansion event, date of capture,

carapace width, sex, and molt conditions (Yamada et al., 2021). Size-structured mark-recapture data (D3) were included to inform trap capture rate parameters of Fukui traps. These data were collected as part of a mark-recapture experiment in July - November 2024 at Roche Cove on Vancouver Island in British Columbia, Canada. Here, crabs were captured and marked, released, and recaptured over several time points.

More information on all three datasets can be found in Appendix 1.

3.3 Model description

We start by detailing the overall state-space IPM^2 model, including the process and observation sub-models (Figure 1). Description of all model parameters can be found in Table 1.

3.3.1 Process model

The process model describes how the population at Drayton Harbor changes through time due to growth, natural mortality, removal, and annual recruitment (Figure 1A). The following process equations describe the integral projection model that uses a kernel to project the population forward in time based on seasonal size-dependent growth and size-dependent natural survival (Rees et al., 2014). Over the winter between years (November - March; Figure 1A), size-dependent natural survival in the kernel becomes density-dependent. We then describe the annual recruitment process and how the time series is initialized with the first population density. These equations detail how the population changes during the trapping season (intra-annual change; April - October) and during the winter season (inter-annual change; November - March) (Figure 1A). The model tracks the state of the population in terms of its distribution of carapace sizes, $N_{t,y}(x)$, which is the density function of individuals of size x during year y at time t. We use a two-week time interval between t and $t+1$, and we incorporate environmental stochasticity as growth variation at each time step, as well as demographic stochasticity in density-dependent overwinter mortality.

Integral projection model

The population density by size, $N_{t,y}(x)$, is projected forward in time using an integral projection model. The integral projection model is discrete in time and continuous over size x, and for estimation, the abundance of individuals is discretized using a small size interval ($\Delta x = 5$ mm). The total population size, $N_{t,y}$, is $\int_{x\in\Omega} N_{t,y}(x)dx$, where Ω represents all biologically feasible sizes (0 - 110 mm).

A kernel, $K_t(x', x)$, describes the probability density of moving from size x to size x' at time t. $N_{t+1,y}(x)$ is therefore a function of $N_{t,y}(x)$, $K_t(x', x)$, the total count of removed crabs in each time period, $C^T_{t,y}(x)$, and recruit abundance, $R(x)$. Recruits annually enter the model at one time point, t_R, where I is a binary

variable indicating whether $t = t_R$:

$$N_{t+1,y}(x') = \int_{x' \in \Omega} K_t(x', x)(N_{t,y}(x) - C^T_{t,y}(x))dx + R(x)I_{t=t_R} \quad (1)$$

The kernel is defined as the product of a growth kernel, $G_t(x', x)$ and size-dependent natural survival, $S(x)$:

$$K_t(x', x) = G_t(x', x) \times S(x) \quad (2)$$

Seasonal growth

Like many ectotherms, green crab growth is strongly seasonal, with the growth rate peaking in the summer due to seasonal variation in temperature, light, and food availability (Contreras et al., 2003; García-Berthou et al., 2012). We therefore use a seasonal growth model that modifies the traditional von Bertalanffy growth model to incorporate seasonal growth oscillations by including a sine function with a period of one year (Beverton & Holt, 2012; Somers et al., 1988). The below growth equation describes growth from the theoretical age of a crab when it is of size 0, d_0, to the expected size of a crab at age a, $\widetilde{W(a)}$. Here, x_∞ is the asymptotic average size, k is a measure of the exponential rate of approach to the asymptotic size, A modulates the amplitude of the growth oscillations, and d_s is the time (fraction of a year) between $t = 0$ (April) and the start of the convex portion of the sinusoidal growth oscillation (i.e., inflection point) (García-Berthou et al., 2012). Note that the d_0 parameter is not of biological interest and is instead an important modeling artifact commonly used to adjust the model for the initial size of the animal, as most fitted models do not pass through the origin (García-Berthou et al., 2012; Schnute & Fournier, 1980).

$$\widetilde{W(a)} = x_\infty(1 - \exp(-k(a - d_0) - s(a) + s(d_0))) \quad (3)$$

$$s(a) = \frac{Ak}{2\pi}\sin(2\pi(a - d_s)) \quad (4)$$

However, since the age of the captured crabs in the multi-year time series dataset (D1) is unknown, we use an equation to describe incremental growth from size x to x' derived from Equation 3 (White et al., 2016). Here, d_t and d_{t+1} are the year fraction associated with t and $t + 1$ (i.e., $d_t = 0$ for Julian day 91, $d_t = 0.5$ for Julian day 274), and $\mu^G_{x,t+1}$ is the mean size at $t + 1$, given x at t.

$$\mu^G_{x,t+1} = x + (x_\infty - x)(1 - \exp(-k\Delta t - s(d_{t+1}) + s(d_t)) \quad (5)$$

Using the large sample approximation, we distribute individuals following a normal distribution across

sizes. The growth kernel, $G_t(x', x)$, is therefore described as:

$$G_t(x', x) = \phi(x'; \mu^G_{x,t+1}, \sigma^2_G) \tag{6}$$

where σ_G is the standard deviation in the growth rate and ϕ is the normal probability density function. The kernel is also normalized such that $\sum_{x' \in \Omega} P(x'|x) = 1$ for each x.

Natural mortality

The rate of natural mortality decreases with size, as smaller crabs have lower intra- and inter-specific competitive abilities and are more susceptible to predation and cannibalism (Grosholz et al., 2021; Maszczyk & Brzezinski, 2018). Natural survival during the non-winter season, S, is described as:

$$S(x) = \exp\left(-\Delta t(\beta + \frac{\alpha}{x^2})\right) \tag{7}$$

where β is the unitless intensity of size-independent natural mortality, and α (which has units of length) is a scalar that modulates the intensity of size-dependent natural mortality (Carlson et al., 2010).

Overwinter growth and density-dependent mortality

To transition from the last time point, $t_{\max}$, in year y to the first time point in year $y + 1$, the population density experiences seasonal growth and density- and size-dependent overwinter mortality.

The size distribution after seasonal growth and before overwinter mortality, $M_y(x)$, is a function of the total population density at the onset of winter $N_{t_{\max},y}(x)$, the total count of removed crabs at the onset of winter $C^T_{t_{\max},y}(x)$, and the overwinter growth kernel $G^o(x', x)$. Here, $G^o(x', x)$ follows the same incremental seasonal growth described in Equation 5, except d_t and d_{t+1} are replaced with the year fraction associated with the onset of winter, $d_{t_{\max}} = 0.53$, and the first time point in the following year, $d_1 = 0$.

$$M_y(x) = \int_{x' \in \Omega} G^o(x', x)(N_{t_{max},y}(x) - C^T_{t_{max},y}(x))dx \tag{8}$$

Due to thermal stress and starvation, the intensity of overwinter mortality is likely stronger than other times of the year and plays an important role in population regulation through density-dependent control on population size (Henderson et al., 1988). Overwinter mortality is also size-selective; smaller animals tend to have lower energy reserves than larger animals and use reserves more rapidly due to the allometry of metabolic rate (Hurst, 2007). Probability of overwinter survival, S^o, is therefore modeled as a density-size interaction, such that the intensity of size-dependent overwinter mortality increases at higher population

densities.

$$S_y^o(x, N_{t_{\max},y}) = \exp\left(-(\frac{\alpha^o \times N_{t_{\max},y}}{x^2} + \epsilon_y)\right) \tag{9}$$

Process error enters as a year-specific overwinter mortality random effect, with standard deviation, σ_o.

$$\epsilon_y \sim \text{Normal}(0, \sigma_o) \tag{10}$$

To implement demographic stochasticity during the overwinter mortality process, we discretize the continuous size distibution x to discrete size intervals x_i. The abundance of crabs in each size interval surviving the winter, $\tilde{N}_{1,y+1}(x_i)$, is drawn from a binomial distribution, where the number of trials is the rounded abundance of crabs after seasonal growth in each size interval, $\tilde{M}_y(x_i)$, and the probability of success is the probability of overwinter survival, $S_y^o(x_i)$. More information about the discretization can be found in the Observation Model section below.

$$\tilde{N}_{1,y+1}(x_i) \sim \text{Binomial}\left(\tilde{M}_y(x_i), S_y^o(x_i, N_{t_{\max},y})\right) \tag{11}$$

Since density-dependence during overwinter mortality plays an important role in long-term population dynamics, we performed a model selection procedure to test a variety of formulations for Equation 9 (further described in the Model Fitting section below).

Initial population density and annual recruitment

To initiate the process model time series, we estimate the size distribution and density of adults at the beginning of the first year. We also estimate the size-structured abundance of recruits that enter the process model each year.

The first size distribution, $N_{1,1}(x)$, is defined in terms of the abundance of adults in the first time period during the first year, λ^A, the log-mean initial adult size in millimeters, μ^A, and the log-standard deviation of initial adult size in millimeters, σ^A. Since the first year of multi-year time series data (D1) in 2020, $y = 1$, was at the start of green crab establishment in Drayton Harbor, we expected the size distribution to be dominated by age-one crabs with a few age-two crabs representing the first cohort of colonizing crabs. We therefore assumed a log-normal initial density to allow for a unimodal size distribution with a longer right tail. Here, ϕ_L represents the log-normal probability density function.

$$N_{1,1}(x) = \phi_L(x; \mu^A, \sigma^A) \times \lambda^A \tag{12}$$

Ovigerous females spawn in August-December (Klassen & Locke, 2007), and these planktonic larvae exit estuarine habitat to develop in high salinity coastal waters alongside larvae produced by neighboring habitats. Advection then brings larvae back into the estuary during recruitment (Young & Elliott, 2019). Recruitment is therefore modeled as an annual event with open demography, where the annual abundance of recruits, λ_y^R, is independent of adult abundance and follows a log-normal distribution

$$\lambda_y^R \sim \text{Log-normal}(\mu^\lambda, \sigma^\lambda) \tag{13}$$

The annual size distribution of recruits, $R_y(x)$, is defined in terms of the annual abundance of recruits, λ_y^R, the mean initial recruit size in millimeters, μ^R, and the standard deviation of initial recruit size in millimeters, σ_R. ϕ represents the normal probability density function.

$$R_y(x) = \phi(x; \mu^R, \sigma_R^2) \times \lambda_y^R \tag{14}$$

Most crabs will settle from their planktonic larval stage in January to April (Yamada et al., 2005). Instead of estimating the time of planktonic settlement, we represent the recruits annually entering the population at a time point, t_R, (Equation 1) when 1) it can be assumed that the larvae have already settled as juveniles (i.e., mean initial recruit size, μ^R, is greater than zero) and 2) well before the recruits grow into an observable size (Figure 1B). The recruits therefore enter the process model in mid-May, corresponding to $t_R = 6$.

3.3.2 Observation model

The observation equations describe the data-generating process for the three datasets. A removal model was used to describe how the multi-year time series data (D1) relates to the latent abundance, $N_{t,y}(x)$, at Drayton Harbor. Harvest mortality through trapping is described as a size-selective hazard rate, which is informed by both the multi-year time series data (D1) and mark-recapture data (D3). The seasonal growth process was informed by the multi-year time series data (D1) and size-at-age data (D2).

The process model equations in section 3.3.1 describe the latent population dynamics at Drayton Harbor (D1), including the latent states, overwinter mortality, initial population density, and recruitment process (Figure 2). Other process parameters, including the seasonal growth and natural mortality parameters, were informed by multiple datasets (Table 1, Figure 2). Below we also describe how D2 and D3 inform the shared parameters in the process equations (Figure 2).

To facilitate estimation of the IPM^2 parameters, the latent abundance, $N_{t,y}(x)$, is discretized using a grid of values $x_i, \ldots, x_m$ that are regularly spaced such that $\Delta x = 5$ mm and $m = 22$. The discrete latent abundance, $\tilde{N}_{t,y}(x_i)$, is approximated in kernel transitions by the midpoint rule, where $\tilde{N}_{t,y}(x_i) =$

$\int_{x_i-\frac{\Delta_x}{2}}^{x_i+\frac{\Delta_x}{2}} N_{t,y}(x)dx$.

Removal observation process (D1)

A removal model was used to describe the data-generating process for the time series data at Drayton Harbor (D1, Figure 1). Here, the removal count data, $C_{t,j,y}(x_i)$, represent the number of crabs of size x_i, caught at time t, during year y, in trap j, conditioned on the discrete size-structured latent abundance, $\tilde{N}_{t,y}(x_i)$ (Kéry & Royle, 2015). Multiple traps were placed simultaneously in each time period, so we factor the probability of the removal count data in one time period as 1) a binomial distribution for the total number of removed crabs, $C^T_{t,y}(x_i)$ across all traps and 2) a Dirichlet-multinomial distribution for the trap-specific count, $C_{t,j,y}(x_i)$, describing which traps the crabs are caught in, given $C^T_{t,y}(x_i)$. Here, $C^T_{t,y}(x_i) = \sum_j C_{t,j,y}(x_i)$.

The total number of removed crabs, $C^T_{t,y}(x_i)$, follows a binomial distribution with number of trials equal to the discrete latent total abundance of crabs, $\tilde{N}_{t,y}(x_i)$, and total capture probability across all traps set during the same time period, $p_{t,y}(x_i)$.

$$C^T_{t,y}(x_i) \sim \text{Binomial}(\tilde{N}_{t,y}(x_i), p_{t,y}(x_i)) \tag{15}$$

The vector size-structured count of crabs in each trap j, $\mathbf{C}_{t,y}(x_i) = (C_{t,1,y}, \ldots, C_{t,J,y})$, follows a Dirichlet-multinomial mixture distribution with overdispersion parameter, ρ, and a vector of conditional probabilities of capture in trap j, $\mathbf{p^C}_{t,y}(x_i) = (p^C_{t,1,y}, \ldots, p^C_{t,J,y})$. Since the trap compositional data are overdispersed due to green crab aggregation and spatial behaviors, the Dirichlet allows for greater variance in the count data than predicted by a multinomial distribution (Thorson et al., 2017). More information on the Dirichlet-multinomial mixture can be found in Appendix 2.2.

$$\mathbf{C}_{t,y}(x_i) \sim \text{DirichletMultinomial}(C^T_{t,y}(x_i), \mathbf{p^C}_{t,y}(x_i), \rho) \tag{16}$$

Size-selective hazard rates (D1 and D3)

Removal through trapping occurs in continuous time, described as a size-selective hazard rate, $H(x)$, representing the instantaneous intensity of capture (Ergon et al., 2018). The shape and magnitude of this size-selective hazard rate varies among the three trap types used for removal: Fukui, Minnow, and Shrimp traps. Both the time series count data (D1) and mark-recapture data (D3) inform the size-selective probability of capture of Fukui traps, and only D1 informs the size-selective probability of capture of Minnow and Shrimp traps (Figure 2).

Fukui and Shrimp traps capture larger crabs at higher rates than smaller crabs. The respective hazard

rates of Fukui and Shrimp traps, $H_F(x)$ and $H_S(x)$, are modeled as a logistic function of crab size:

$$H_F(x) = \frac{h_F^{\max}}{1 + \exp\left\{-h_F^k(x - h_F^0)\right\}} \tag{17}$$

$$H_S(x) = \frac{h_S^{\max}}{1 + \exp\left\{-h_S^k(x - h_S^0)\right\}} \tag{18}$$

The Minnow trap mesh size is smaller than the maximum crab size, so this trap's size-selective hazard rate, $H_M(x)$, follows a bell-shaped curve (Jørgensen et al., 2009):

$$H_M(x) = h_M^{\max} \times \exp(\frac{x - h_M^A}{2h_M^\sigma}) \tag{19}$$

Each baited trap, j, is placed in the habitat for a short (∼24-48 hr) time interval, $\Delta b_{t,j,y}$. The total capture probability, $p_{t,y}(x)$, is a function of the integrated hazard rate, summed across all traps set during the same time period, $O_{t,y}$.

$$p_{t,y}(x) = 1 - \exp\left(-\sum_{j=1}^{O_{t,y}} H_{t,j,y}(x)\Delta b_{t,j,y}\right) \tag{20}$$

The conditional probability of capture, $p^C_{t,j,y}(x)$, is then $H_{t,j,y}(x)/\sum_{j=1}^{O_{t,y}} H_{t,j,y}(x)$.

Size-at-age observation process (D2)

The size-at-age data, $W_{z,y}(a)$, indicate the carapace width of crab z at age a in year y. Since the age of the crabs in this dataset are recorded, unlike the time series dataset (D1), the unmodified seasonal growth equation is used that relates the theoretical age of the crab when it is of size 0, d_0, to the expected size of a crab at age a, $\widetilde{W_y(a)}$ (Equation 3). A normally distributed error term, ϵ, is used to account for non-independence among data collected in the same year, since growth rate is likely affected by water temperature, which varies from year-to-year.

$$\widetilde{W_y(a)} = x_\infty(1 - \exp(-k(a - d_0) - s(a) + s(d_0))) + \epsilon \tag{21}$$

To account for variation in growth rate, the observed size-at-age data, $W_{z,y}(a)$, follow a normal distribution, with the expected carapace width $\widetilde{W_y(a)}$, and standard deviation, σ_w.

$$W_{z,y}(a) \sim \text{Normal}(\widetilde{W_y(a)}, \sigma_w) \tag{22}$$

Mark-recapture observation process (D3)

The mark-recapture data (D3) primarily informed the observation parameters that describe the size-selective hazard rates of the Fukui trap type, $H_F(x)$ (Equation 17, Table 1, Figure 2), but also components of the growth and natural mortality kernel (Table 1; Figure 2). The mark-recapture data consists of 1) $m_t^{\text{mc}}(x_i)$, the count of marked and released crabs of discrete size x_i for $t \in \{0 \dots t_{\max}^{\text{mc}} - 1\}$ and 2) $r_t^{\text{mc}}(x_i)$, the count of recaptured and released crabs of discrete size x_i for $t \in \{1 \dots t_{\max}^{\text{mc}}\}$ (Appendix 1.3).

The count of marked and released crabs at $t = 0$, $m_0^{\text{mc}}(x_i)$, underwent seasonal growth and natural mortality to the first recapture time period, $t = 1$, where $N_1^{\text{mc}}(x_i)$ is the total marked crabs at $t = 1$.

$$N_1^{\text{mc}}(x_i') = \int_{x \in \Omega} K_0^{\text{mc}}(x', x) m_0^{\text{mc}}(x_i) dx \tag{23}$$

The total number of marked crabs, $N_t^{\text{mc}}(x_i)$, in the remaining recapture time periods $t \in \{2 \dots t_{\max}^{\text{mc}} - 1\}$ undergo seasonal growth and natural mortality:

$$N_{t+1}^{\text{mc}}(x_i') = \int_{x \in \Omega} K_t^{\text{mc}}(x', x)(N_t^{\text{mc}}(x_i) + m_t^{\text{mc}}(x_i)) dx \tag{24}$$

The count of recaptured and released crabs, $r_t^{\text{mc}}(x_i)$, are drawn from a binomial distribution where the size is the total number of marked crabs, $N_t^{\text{mc}}(x_i)$, and probability, $p_t^{\text{mc}}(x_i)$:

$$r_t^{\text{mc}}(x_i) \sim \text{Binomial}(N_t^{\text{mc}}(x_i), p_t^{\text{mc}}(x_i)) \tag{25}$$

where $p^{\text{mc}}(x_i)$ is the total probability of capture based on the total number of Fukui traps set, O_t^{mc}, over the time period Δb^{mc}:

$$p_t^{\text{mc}}(x) = 1 - \exp\left(- \sum_{j=1}^{O_t^{\text{mc}}} H_{F,j}(x) \Delta b^{\text{mc}} \right) \tag{26}$$

3.4 Model fitting

All three datasets were combined in a fully integrated model for joint estimation of model parameters. We fit the IPM^2 in a Bayesian framework using NIMBLE v.1.2.1 (de Valpine et al., 2017). We used vague priors for all parameters, which are provided in Appendix 2.1. Parameters were estimated by running four Markov chain Monte Carlo (MCMC) chains of 100 000 iterations, thinned by a factor of 10. Of these 10 000 samples, 2 000 were discarded as burn-in. We used visual inspection of the MCMC chains and the Brooks and Gelman diagnostic $\hat{R}$ to assess model convergence, and we found that all parameters had an $\hat{R} \leq 1.1$

(Brooks & Gelman, 1998). All analyses were conducted in R version 4.4.1 (R Core Team, 2024). Code for the entire model is provided in Appendix 3, and generic, modular code that closely follows the model description is provided in Appendix 4. Posterior summaries, as well as convergence diagnostics and trace plots of model parameters can be found in Appendix 5.

To assess model performance and robustness, we conducted both a model selection and a model checking procedure (Conn et al., 2018). For model selection, we evaluated multiple functional forms of overwinter mortality using Watanabe–Akaike information criterion (WAIC). The inter-annual population transitions (i.e., transition from year y to year $y + 1$) are largely described by density-dependent overwinter mortality. Since density dependence only enters the model during this process and is therefore likely influential for forecasting the stable size distribution, we compared multiple functional forms for size- and density-dependent overwinter mortality and used the formulation with the lowest WAIC in the final analysis (Eq. 9, Appendix 6.1).

To check the model, we calculated posterior predictive p-values using deviance as an omnibus discrepancy function and proportion of zeros as a targeted discrepancy function to check for zero inflation of the count data (Appendix 6.2). We found that the model was an adequate representation of the data-generating process, with a p-value of 0.43 for the omnibus deviance discrepancy (Appendix 6.2; Figure A6.1). However, the p-value for the proportion of zeros discrepancy function was 0.95, suggesting potential model bias (Appendix 6.2; Figure A6.2). These p-values may be conservative, however, as Bayesian p-values tend to be biased toward 0.5 (Conn et al., 2018).

3.5 Population forecasts

To evaluate the long-term response of a green crab population to varying removal efforts, we approximated the stable size distribution and equilibrium abundance through stochastic forward simulations with posterior samples. Characterizing the equilibrium abundance is most relevant in this context, as the green crab population is considered fully open and sustained local extinction is therefore unlikely. We randomly selected 1000 samples from the full posterior, and for each posterior sample, we generated an initial adult population size and projected the population forward 25 years, applying varying removal efforts for each set of 1000 simulations. These varying removal efforts included a total of 0, 112, 560, and 2800 annual Shrimp, Fukui, or Minnow traps, applied evenly over the trapping season of 14 biweeks (12 total sets of 1000 simulations; four removal efforts x three trap types). Year-varying recruit abundance and size- and density-dependent overwinter mortality were drawn stochastically from process noise distributions each year in the forward simulations (Table 1). To reduce simulation noise between removal effort and trap type combinations, the

same set of process noise stochastic draws for each posterior sample was consistent across the 12 simulation sets.

For each simulation, the size-structured abundance at the end each of year after overwinter mortality, $N_{1,y+1}(x)$, was recorded (Figure 1A). Simulation outputs were summarized as the mean size-structured abundance at the end of years 6-25, with the first five years treated as transient. We removed this transient period from the simulation summaries, since our objective was to characterize the long-term response to different magnitudes of trapping, rather than the temporal dynamics as a population goes from untrapped to a new stable size distribution in response to trapping.

4 Results

4.1 Estimating population-level quantities

The integrated integral projection model tracked the size-structured European green crab abundance at Drayton Harbor (D1) throughout 2020-2023. Figure 3 shows the population density of adults and recruits at the beginning of each year. As the invasion progressed from 2020 to later years in 2021-2023, the size structure of adults shifted toward larger individuals (Figure 3A). This shift was particularly prominent in 2022 as a result of the low recruitment event in 2021, whereas the adult size distributions in 2021 and 2023 were more bimodal as a result of the large recruit age class in 2020 and 2022, respectively, that survived the winter but had not yet grown in size to match the sizes of crabs older than one year. This increase in median adult crab size after 2020 coincided with a decrease in overall adult crab abundance: total adult crab abundance decreased from 438 (358-524 95% CrI) individuals in 2020 to 280 (255-312 95% CrI), 168 (154-184 95% CrI), and 175 (159-195 95% CrI) in 2021-2023.

The abundance of recruits varied by multiple orders of magnitude across years, ranging from 694 (324-1150 95% CrI) and 1381 (841-2021 95% CrI) in the strong recruitment years of 2020 and 2022, to 50 (29-75 95% CrI) and 61 (39-108 95% CrI) in the weak recruitment years of 2021 and 2023 (Figure 3B). The mean size of recruits when they enter the model at $t = 6$ each year (mid-May) was 5.4 (1.0-9.8 95% CrI) millimeters (Figure 3B; Appendix 5). The credible intervals around recruit abundance and size are large (Figure 3B), since these recruits are unobserved until they grow into the observable size range in August - September (Figure 1B).

4.2 Distinguishing size-structured natural and harvest mortality

By combining information in multiple datasets, the integrated population model allowed for estimation of additional parameters – size-structured natural and harvest mortality – that were not identifiable with any one component dataset (Riecke et al., 2019).

Removal rates were estimated for three trap types – Fukui, Shrimp, and Minnow – with different rates of removal and size selectivities (Figure 4). Overall, Shrimp traps removed crabs at the highest rate, and Minnow traps were only effective at removing crabs in the 30-60 mm size range. No trap effectively removed crabs smaller than 30 mm, consistent with the completely unobserved small crab portion of the population (Figure 1B).

Natural survival rates over the five winter months were lower than natural survival rates during the seven other non-winter periods of the year (Figure 5), consistent with the expectation that density-dependence in overwinter mortality plays an important role in population regulation. Model comparison with WAIC demonstrated support for overwinter mortality as a function of the interaction between individual crab size and total population density (Appendix 6.1, Eq. 9). Overwinter survival rates varied significantly from year to year, and correlated with total abundance and recruitment strength. Years with higher overall population density coincided with particularly low overwinter survival of small crabs (Figure 5B). In response to large recruitment events in 2020 and 2022 (Figure 3), over the winter following these years, survival rates dropped to 0.75 for crabs of the largest size and less than 0.25 for crabs of smaller size (Figure 5B). Conversely, survival rates were high over the winter between 2021 and 2022 in response to a small recruitment event in 2021 (Figure 3B) and an adult size structure biased toward larger crabs (Figure 3A).

4.3 Isolating growth in body size as a time- and size-dependent process

Isolating the contribution of growth in body size in individuals to changes in population size structure helped facilitate inference of other size-structured demographic rates. This growth rate was strongly seasonal and varied throughout the year, with growth rate peaking in the summer months and approaching zero in the winter months (Figure S1). The inflection point of the sinusoidal growth oscillation, d_s, indicates the time of year when body growth is most rapid. Since d_s was 0.25 (0.21 - 0.28 95% CrI), and $d_t = 0$ corresponds to April 1st (Julian day 91), the fastest rate of growth occurs around July 1st. The mean asymptotic crab size, x_∞ was 80.7 mm (78.9-82.5 95% CrI) (Appendix 5). Growth was also variable; the standard deviation in growth rate, σ_G, was 2.8 mm (2.3-3.2 95% CrI) (Figure S1).

4.4 Population forecasts

Stochastic forward simulations with posterior samples were used to forecast the stable size distribution and equilibrium abundance under different levels of removal effort, and subsequently different levels of harvest mortality (Figure 6). These simulations indicated that a low removal effort with Fukui and Minnow traps (Figure 6B-C) resulted in only marginal changes in the stable size distribution and equilibrium abundance relative to no removal effort (Figure 6A, Table S1). For example, the mean total equilibrium abundance, $N^E = \int_{x \in \Omega} N^E(x)dx$, across simulation replicates with no removal was 270 crabs (Table S1). While the mean N^E across simulation replicates with 2800 annual Fukui and Minnow traps was 239 and 210, respectively (Table S1). With a high removal effort of Shrimp traps, the total equilibrium abundance, N^E, decreases to 64 crabs, and large adult crabs can be completely removed from the population (Figure 6D, Table S1). However, this large crab removal merely shifts the stable size distribution toward smaller crabs; the equilibrium abundance of smaller crabs actually increases relative to no removal effort (Figure 6; Figure S2).

5 Discussion

Our integrated integral projection model (IPM^2) – a framework first described by Plard et al. 2019 – provides important insight for how body size can modulate many individual-level demographic rates that interact to describe population-level dynamics (Plard et al., 2019). The IPM^2 produces an outcome greater than the sum of its parts: combining information in multiple datasets facilitates population inference for a species with complex demography with imperfect measurements. We are able to disentangle multiple size-structured demographic rates that simultaneously change the size distribution over time (Carlson et al., 2010; Sogard, 1997), allowing detailed understanding of the individual contributions of each size-structured demographic rate to overall population dynamics. These results also fill a significant knowledge gap for invasive European green crab (*Carcinus maenas*). While the species is highly studied due to its geographic ubiquity and management concern, this study is the first to quantify removal rates and size-structured population abundance (Young & Elliott, 2019), providing a path forward for assessing feasibility of control and optimizing management actions.

5.1 Disentangling size-structured demographic rates

The IPM^2 provides novel insights into previously uncharacterized size-structured European green crab demographic rates, including size-structured natural mortality, size- and density-dependent overwinter mortality, recruitment processes, size-structured growth rate, and size-selective harvest rates.

The model estimates unobserved quantities, most notably the abundance and size (carapace width) of recruits before they grow into observable size classes (Figure 1B, Figure 3). Due to the size-selectivity of most observation and removal methods, very little is known about early stages of the green crab life cycle (Yamada et al., 2005), yet here, we used growth rates estimated by larger sizes to back-calculate size and abundance of recruits before they are observed. However, the model may underestimate non-overwinter natural mortality at smaller sizes, and therefore recruit abundance, because after settlement from the planktonic phase, recruits are unobserved for months and are likely dying naturally at very high rates (Figure 5A). Previous studies have reported extremely high densities of small juveniles (200-2000/m^2) when counting individuals within quadrats in the intertidal zone at low tide where most juveniles are found (Breteler, 1976; Thiel & Dernedde, 1994). To better understand size-dependent, non-winter natural mortality, trap data could be integrated with measurements of small crabs made by other means, like visual or quadrat surveys.

Overwinter mortality is a major size-selective process, as both energy reserves and metabolic rate scale with body size, such that larger individuals have higher energy reserves but lower metabolism and are therefore more resilient to starvation and physical extremes (Carlson et al., 2008; Sogard, 1997). Our results are consistent with this size-dependent mortality pattern, and provide support for the hypothesis that crab size and overall population density interact to modulate overwinter mortality (Appendix 6.1). Overwinter mortality varied significantly from year to year, and years with higher overall population density coincided with particularly low overwinter survival of small crabs (Figure 5B). Overwinter mortality therefore likely plays an important role in regulating size-structured green crab population dynamics (Henderson et al., 1988).

Recruitment varies by orders of magnitude from year to year, ranging from about 50 recruits in weak years to 1000-2000 in strong years (Figure 3B). The green crab has a long planktonic larval stage, living in open marine waters for months before advection back into the estuarine environment where they settle in the sub- and inter-tidal zone (Yamada, 2001). This inter-annual variability in recruitment is consistent with varying oceanographic conditions; the survival and successful transport of larvae often coincide with warm winter water temperatures and oceanographic conditions like El Niño/Southern Oscillation (ENSO) and Pacific Decadal Oscillation (PDO) events (Yamada et al., 2021). For example, the first large green crab colonization event at Drayton Harbor is linked to the 2018-2019 El Niño. These recruits would then grow throughout the year in 2019 to be associated with the high year-one adult abundance observed in 2020 (Figure 3A). Though drawing from a small sample size of only four years, recruit abundance appears to be decoupled from adult abundance; for example, adult abundance was highest in 2020, yet recruit abundance was lowest in 2021 (Figure 3). This decoupling of recruit and adult abundances suggests that recruitment is likely driven by oceanographic conditions and regional population dynamics, rather than local adult abundance.

However, a longer time series coupled with genomic information will be necessary for understanding the relative contribution of local and regional processes in population dynamics.

The model also estimates demographic rates that vary across time and size. Marine invertebrates are often subject to seasonal variation in environmental factors like photoperiod, food availability, and temperature, resulting in elevated rates of growth, feeding, and oxygen consumption in the summer season (Brockington & Clarke, 2001). Consistent with this expectation, we find that green crab growth is strongly seasonal, with growth rate peaking in summer months and approaching zero in the winter (Figure S1). Green crab growth rate is also size-dependent, as the molting rate is much higher at smaller crab sizes, and slows down as crabs approach the mean asymptotic crab size (Yamada et al., 2005).

The IPM^2 estimates absolute size-selective capture rates for different trap types, allowing for the first estimates of size-structured abundance of European green crab (Young 2020). These capture rate and abundance estimates mark an important advance for moving beyond catch per unit effort (CPUE) as the primary, yet imperfect, method for measuring population trends (Harley et al., 2001). These results also highlight the strong size-selectivity of removal methods, since capture rates approaching zero for crabs smaller than 30 millimeters (Figure 4). This size selectivity will have uncertain evolutionary consequences, yet resolving this uncertainty will be important for projecting long-term population dynamics. Fishing-induced life-history evolution is frequently observed in harvested species (Enberg et al., 2012), and previous invasive species management programs have demonstrated rapid ecological and evolutionary changes in response to selective harvesting, including a shift toward earlier size at maturity and an overall slower growing phenotype (Evangelista et al., 2015). These phenotypic responses to removal programs can have strong effects on ecosystem recovery (Závorka et al., 2020), so understanding the role of green crab removal as a selection pressure will be important for managing this species capable of rapid adaptation (Tepolt & Palumbi, 2020).

5.2 Predicting the impact of removal on European green crab dynamics

These estimates of size-structured demographic rates and size-selective harvest rates will be essential for understanding the impact of removal on green crab dynamics and the feasibility of population suppression. Our model results show that harvest mortality associated with low levels of removal effort, especially with Fukui and Minnow traps, only marginally change the equilibrium abundance and size structure, relative to doing nothing (Figure 6A-C; Table S1). These results highlight that low levels of removal effort can be useful for monitoring population trends but are insufficient for control and population suppression.

Even with extremely high levels of removal effort with the most effective trap type - Shrimp traps - control

will mostly shift the stable size distribution of the population toward smaller crab sizes (Figure 6D; Figure S2). For example, if 2800 Shrimp traps are applied throughout the year, the resulting total equilibrium abundance, N^E, is 25% of the total equilibrium abundance if no traps were set (Table S1), yet the remaining crabs are all <60 mm (Figure 6D). These results are consistent with observations of decreased median carapace width in response to removal (de Rivera et al. 2007), and they support the prediction that though removal programs may achieve short-term or local benefits, control is likely unable to sustainably suppress populations over larger temporal and spatial scales (Kanary et al., 2014; Keller et al., 2025; Tummon Flynn et al., 2024). In fact, strong removal pressure increases the equilibrium abundance of small crabs (Figure 6D, Figure S2). Removing adult crabs reduces the intra-specific regulation of recruits, resulting in higher abundance of smaller crabs relative to doing nothing. This increase in small crab abundance is similar to dynamics observed in an intensive control experiment by Grosholz et al. 2021, the first controlled experimental field demonstration of the "hydra effect" (Grosholz et al., 2021). The ecological outcome of a removal-induced shift in size structure will likely be location-specific and depend upon the impacted species. While the competitive advantage between green crab and native crab species and the rate of predation upon Manila clams and adult Pacific oysters increases with crab size, crab size does not appear to affect the rate of eelgrass alteration and larval Pacific oyster consumption (Anaya et al., 2025; McDonald et al., 2001).

These results are dependent on the assumption of a completely open population, where recruitment rate is independent of the local population size. This assumption, in general and in the case of Drayton Harbor in this study, is likely appropriate, as genomic analyses find high gene flow and low genetic structure across local green crab populations in the Northeast Pacific (Tepolt et al., 2009, 2022). However, these results may not be applicable in some circumstances where a local population is partially closed, often in unique oceanographic conditions that support strong larval retention within an estuary (Grosholz et al., 2021).

The population forecasts assume stationarity when predicting the equilibrium abundance and stable size distributions under varying removal efforts (Figure 6). While these forecasts allow recruitment to vary from year to year, the mean and variance of recruit abundance is constant over time. These forecasts would likely be different if recruitment is non-stationary, either decreasing over time through intensive removal efforts across the region or at known source populations, or increasing over time through increased colonization pressure. Non-stationarity in colonization pressure is likely, as climate and oceanographic models project an increase in oceanographic events that support survival and transport of larvae (Cai et al., 2021; Du et al., 2024). Other demographic rates, like growth and natural mortality may also be non-stationary. The integral projection model lends itself to understanding how changing environmental factors, like increased temperature, will affect individual size and overall population dynamics (Dahlgren & Ehrlén, 2011; Plard et al., 2019).

5.3 Reliability of parameter estimates in integrated population models

Integrated population models are useful for inferring parameters of interest in scenarios where information needs of complex models exceed information in individual datasets. Despite these benefits, often the reliability of parameter estimates remains underexamined. Simulation-based approaches have shown that IPM parameters – particularly "additional", previously unidentifiable parameters – are sensitive to violations of model assumptions (Riecke et al., 2019). In the green crab IPM^2, management-relevant model parameters, including size-structured natural and harvest mortality, were not estimable from one data source but were indirectly estimable from multiple data sources and the assumed model structure. For example, the Roche Cove mark-recapture dataset (D3) was critical for inferring trap hazard rates and abundance estimates at Drayton Harbor where the multi-year time series data was collected (D1).

The IPM assumes that the same ecological process has generated these disparate datasets. Posterior predictive checks that compare the observed data to data generated by the model can be a valuable tool for evaluating violations of this assumption. For example, the deviance-based Bayesian p-value that tests the model's global lack of fit was 0.43 (Appendix 6.2). We also fit the model with an alternate mark-recapture dataset collected at a different location, Seadrift Lagoon in California, USA (Appendix 6.3.1). The habitat at Drayton Harbor (D1) is much more similar to Roche Cove (D3) than to Seadrift Lagoon, and these differences may impact inter- and intraspecific population processes (Appendix 6.3.1). The deviance-based Bayesian p-value calculated with the alternate Seadrift Lagoon mark-recapture data was 0.71 (Appendix 6.3). The p-value of an unbiased model is 0.5, suggesting that inference with Roche Cove (D3) is less biased than inference with the alternative dataset. Posterior predictive checks may be useful for understanding if the multiple datasets reflect the same data-generating process and if disparate datasets can feasibly be combined in an integrated population model.

The targeted posterior predictive check used to assess zero inflation in the count data at Drayton Harbor, $C(x_i)_{t,j,y}$, produced a Bayesian p-value of 0.95. This result suggests that the model may inadequately account for processes that could generate overdispersion in the count data, like spatial heterogeneity in green crab distribution within Drayton Harbor or interactions between traps set simultaneously.

5.4 Embedding the IPM^2 in a decision-making framework

These results demonstrate that removal cannot eradicate an open population of European green crab (Figure 6). While removal can decrease the total equilibrium population size at a location like Drayton Harbor with relatively low colonization pressure (Table S1), removal primarily shifts the stable size distribution toward smaller crabs (Figure 6D). In circumstances where invasive species eradication is infeasible, the management

focus often moves toward functional eradication, or suppression of the population below levels that cause unacceptable ecological effects (Green & Grosholz, 2021). The IPM^2 green crab model may become valuable in a decision-making framework to optimize removal actions and find the removal effort – and subsequently the stable size distribution and equilibrium abundance – that both minimizes removal cost and impact on habitat, native species, and natural resources.

Embedding this size-structured model within a decision-making framework, however, will require improved knowledge of size-structured impacts and computational methods to optimize high-dimensional decision problems. Green crab size often mediates its interactions between prey and competitors; other decapod species are preyed upon by green crab as juveniles but outcompete green crab as adults, and green crab often only predate upon bivalves of smaller size (Curtis et al., 2012; Grosholz, 2005; McDonald et al., 2001; Williams et al., 2009). Quantifying size- or biomass-dependent impacts will be critical for optimizing allocation of removal resources in this size-structured system. Additionally, this work highlights that green crab population dynamics cannot be represented in a one-dimensional system (i.e., total abundance), since the size structure of the population plays an important role in long-term dynamics. Techniques like stochastic dynamic programming can be used to optimize sequential decision problems (Marescot et al., 2013), yet due to the curse of dimensionality, these methods will be insufficient for optimizing problems with large state and action spaces. The size-structured green crab abundance changes within a single decision cycle, and multiple trap types have different size-dependent removal rates and different monetary and logistical costs of use (Figure 3). Since the complexity of the decision problem scales non-linearly with the size of the system, advanced computational methods like neural-network-based reinforcement learning or factored Markov decision processes will be needed to optimize management actions in this high-dimensional decision problem (Lapeyrolerie et al., 2022; Nicol et al., 2015).

6 Tables

Table 1: Notation and biological meaning of data, latent states, and parameters. Category refers to the parameter categories designated in Figure 2: 1) Init is the size structure of initial population density and annual recruits, 2) Growth is seasonal growth, 2) N. mort is size-dependent and size-independent natural mortality in non-winter months, 3) O. mort is size- and density-dependent overwinter mortality, 4) F obs, M obs, and S obs correspond to the size-selective observation process for Fukui, Minnow, and Shrimp traps, respectively, and 5) Pop. size corresponds to the true population size in the state-space model (Figure 1).

Symbol	Description	Category
	Demographic parameters	
μ^A	Log-mean adult size in millimeters at $t = 1$ and $y = 1$.	Init
σ^A	Log-standard deviation of adult size in millimeters at $t = 1$ and $y = 1$.	Init
μ^R	Mean recruit size in millimeters upon entry into the process model at $t = 6$.	Init
σ_R	Standard deviation of recruit size in millimeters upon entry into the process model at $t = 6$.	Init
x_∞	Asymptotic average crab size (carapace width, in mm).	Growth
k	Exponential rate of approach to the asymptotic size.	Growth
A	Parameter modulating the amplitude of seasonal growth oscillations.	Growth
d_s	Time (fraction of a year) between $t = 0$ (April) and the start of the convex portion of the sinusoidal growth oscillation (i.e., inflection point)	Growth
σ_G	Standard deviation of somatic growth.	Growth
d_0	Theoretical age a crab is of size zero millimeters.	Growth
σ_w	Standard deviation of normally-distributed error term to account for heterogeneity in individual growth rates in the size-at-age data.	Growth

σ_y	Standard deviation of normally-distributed error term to account for non-independence among size-at-age data collected in the same year.	Growth
β	Intensity of size-independent natural mortality (not in winter months).	N. mort
α	Scalar that modulates the intensity of size-dependent natural mortality (not in winter months).	N. mort
α^o	Intensity of overwinter density- and size-dependent natural mortality.	O. mort
σ_o	Standard deviation of year-specific overwinter mortality random effect.	O. mort
	Observation parameters	
$h^{\max}$	Maximum harvest mortality hazard rate. Maximum rate is trap type-specific, such that h_F^{max}, h_M^{max}, and h_S^{max} correspond to Fukui, Minnow, and Shrimp traps, respectively.	F Obs, M Obs, S Obs
h^k	Steepness of change from the minimum to the maximum hazard rate for trap types with a logistic size-selective function, such that h_F^k and h_S^k correspond to Fukui and Shrimp traps, respectively.	F obs, S obs
h^0	Midpoint of change from the minimum to the maximum hazard rate for trap types with a logistic size-selective function, such that h_F^0 and h_S^0 correspond to Fukui and Shrimp traps, respectively.	F obs, S obs
h_M^A	Crab size associated with maximum hazard rate with Minnow traps.	M obs
h_M^σ	Width parameter in the Minnow size-selectivity hazard rate function.	M obs

ρ	Parameter that describing overdispersion in the Dirichlet-multinomial mixture distribution.	F obs, M Obs, S Obs
	Population-level quantities	
$N_{t,y}(x)$	Population density function of individuals of size x, during year y, at time t.	Pop. size
$\tilde{N}_{t,y}(x_i)$	Discretized population density of individuals of size x_i, during year y, at time t.	Pop. size
$N_{t,y}$	Total population abundance across all sizes, during year y, at time t.	Pop. size
λ^A	Adult abundance at the first time period, $t = 1$, during the first year, $y = 1$.	Pop. size
λ_y^R	Recruit abundance in year y.	Pop. size
μ^λ	Log-mean recruit abundance.	Pop. size
σ^λ	Log-standard deviation of recruit abundance.	Pop. size
	Observational data	
$C_{t,y}^T(x_i)$	Total count of removed crabs across all traps during time t, in year y, of discrete size x_i in the multi-year time-series dataset (D1).	-
$C_{t,j,y}(x_i)$	Count of removed crabs in time t, in trap j, in year y, of discrete size x_i in the multi-year time-series dataset (D1).	-
$O_{t,y}$	Number of observations (traps) in time t, in year y in the multi-year time-series dataset (D1).	-
$W_{z,y}(a)$	Size of crab z, of age a, during year y in the size-at-age dataset (D2).	-
$m_t^{\text{mc}}(x_i)$	Number of marked and released crabs of discrete size x_i at time t in the mark-recapture dataset (D3).	-

$r_t^{\mathrm{mc}}(x_i)$	Number of recaptured crabs of discrete size x_i at time t in the mark-recapture dataset (D3).	-
O_t^{mc}	Number of observations (Fukui traps) at time t in the mark-recapture dataset (D3).	-

7 Figures

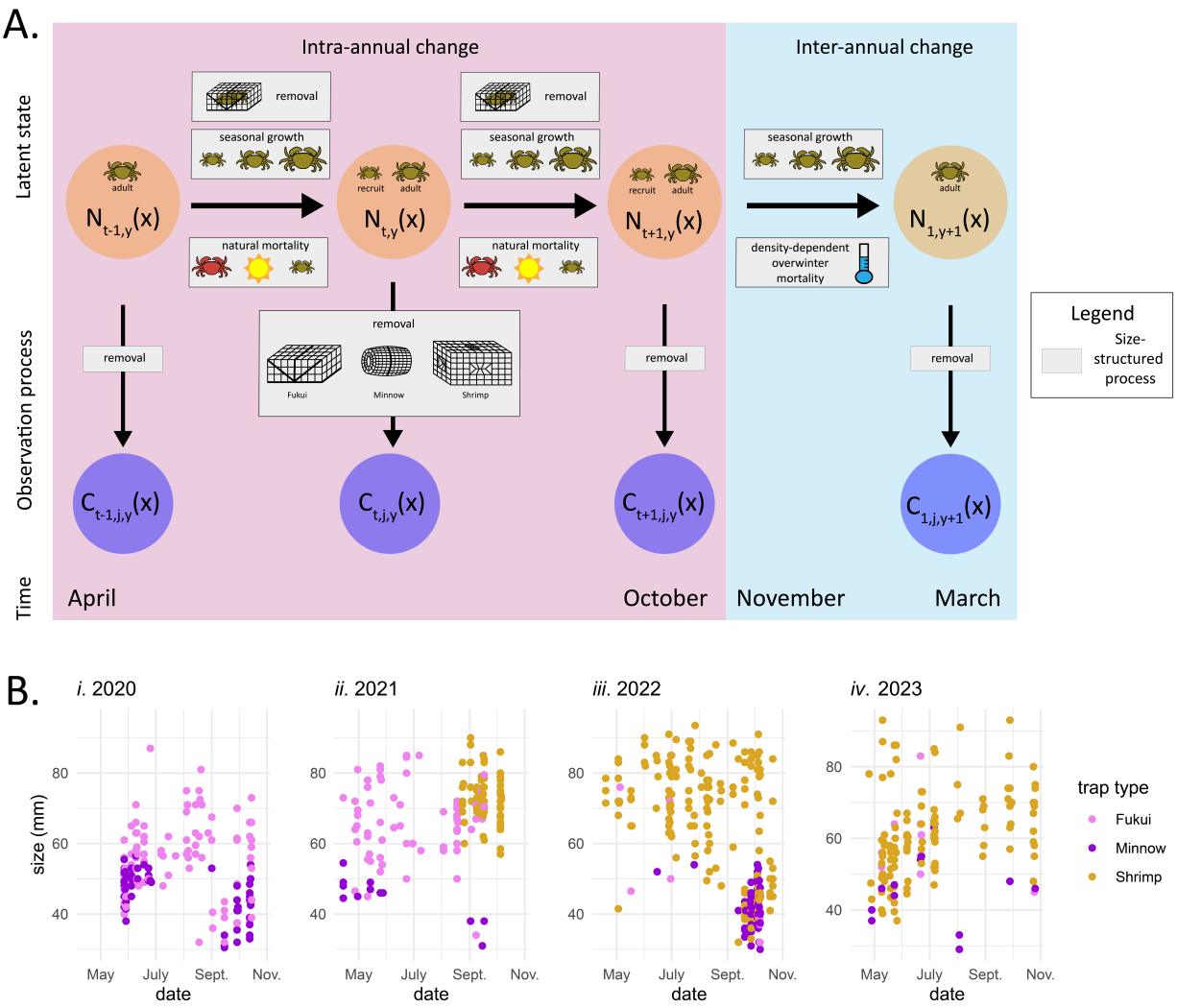

Figure 1: *A.* Conceptual diagram of state-space population model, including the dependence structure in the latent process dynamics and observation process. Orange circles designate the population density of individuals of size x, during year y, at time t and are distinguished by dynamics within a year (intra-annual change, April - October) and dynamics between years (inter-annual change, November - March). Blue circles designate the count of removed crabs during time t, in trap j, in year y, of size x in the multi-year time-series dataset (D1). Grey boxes represent size-structured demographic and observation processes. *B.* Multi-year time series data (D1) collected in Drayton Harbor from 2020-2023, highlighting the relationship between time and crab size (carapace width, mm). Each point corresponds to one captured crab, and color corresponds to the type of trap used in capture.

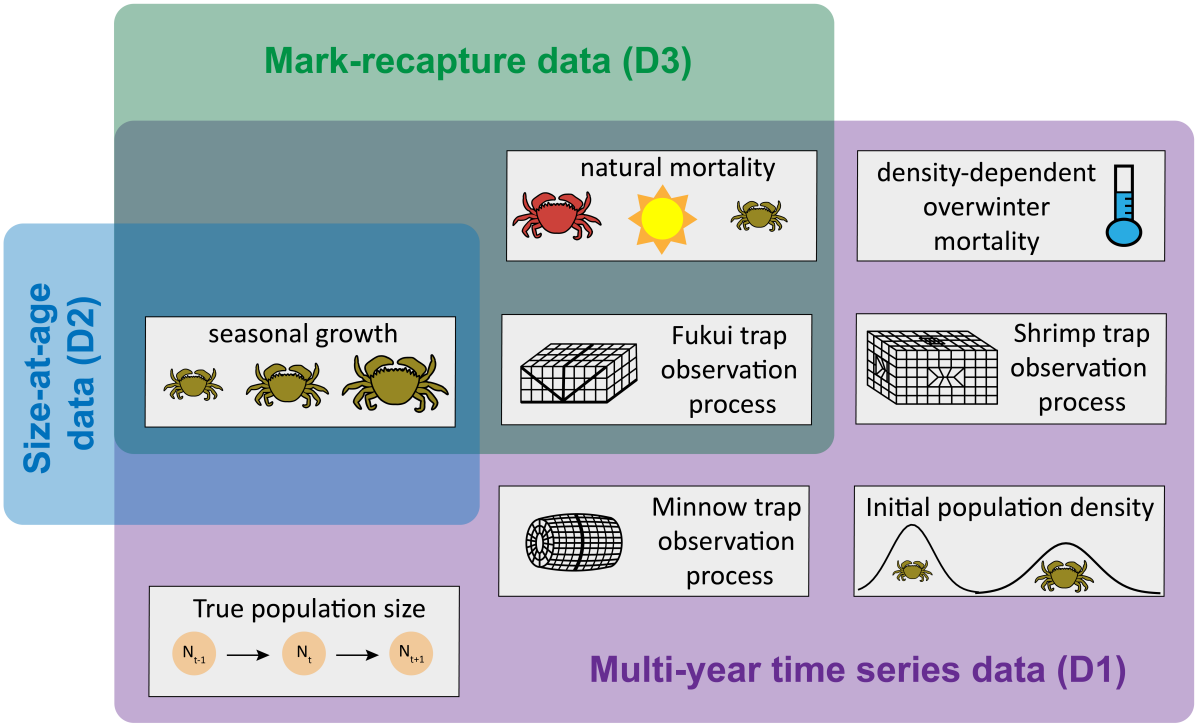

Figure 2: Overview of parameters informed by the three datasets in the integrated population model: multi-year time series data (D1) (Figure 1B), size-at-age data (D2), and mark-recapture data (D3). Parameter categories correspond to categories designated in Table 1.

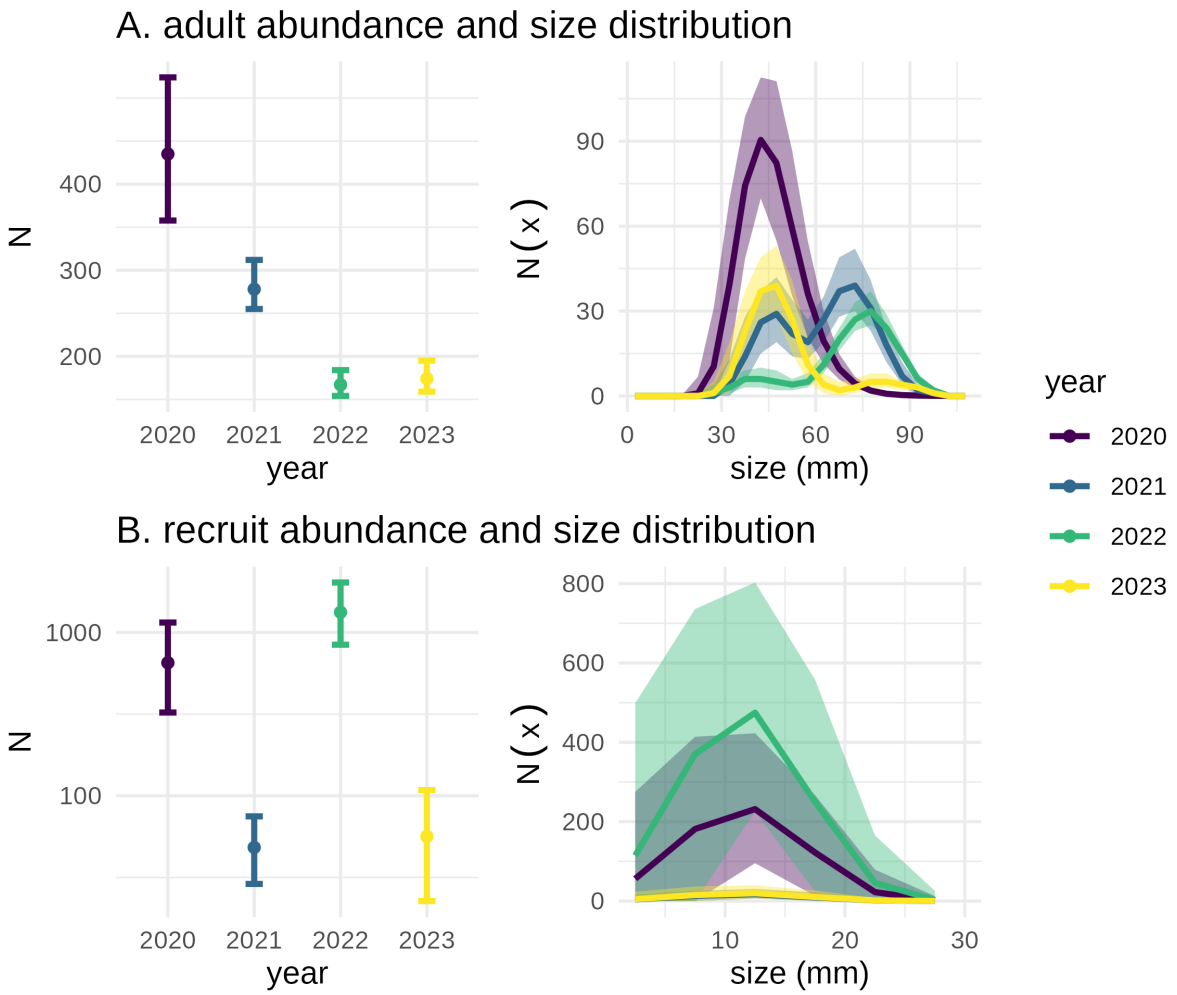

Figure 3: Total abundance and size distribution of *A.* adults and *B.* recruits in the fitted model. The left panels show the total abundance of crabs across all size classes, N, at the beginning of each year (i.e. $N_{1,y}$. The right panels show the size distribution, or the number of individuals in each size class, $N(x)$. Size corresponds to crab carapace width. Colors indicate the year, and error bars indicate the 95% credibility interval. Note that the left panel is the integral of the right panel.

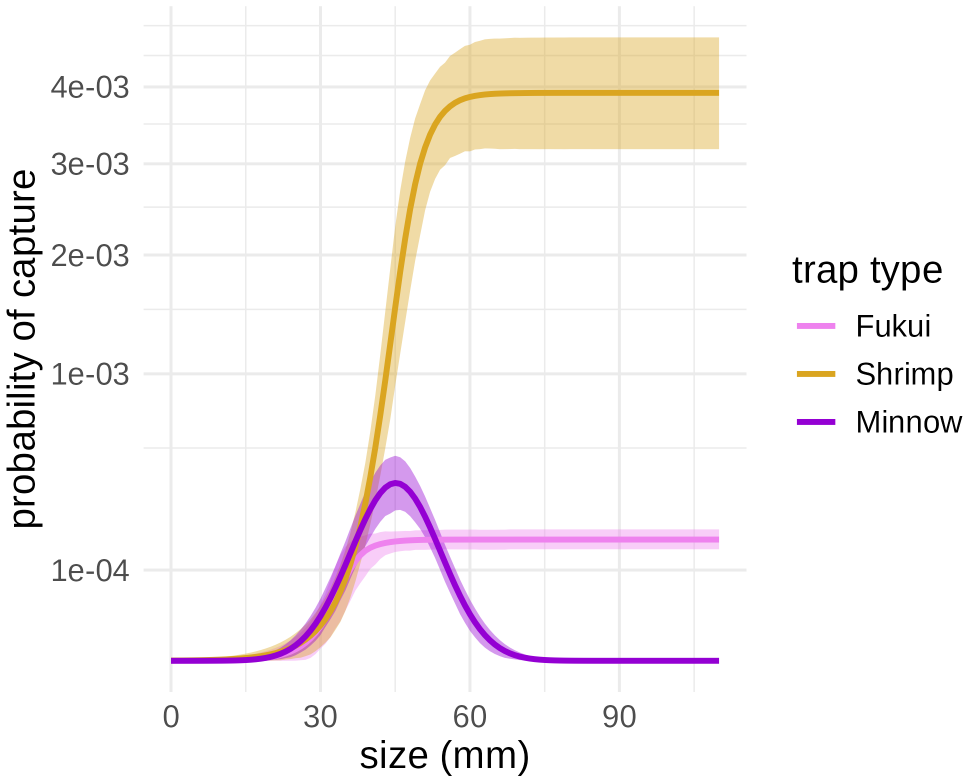

Figure 4: Size-structured probability of capture, $p(x)$, in one trap over a 24-hour trapping period. Colors indicate the trap type. Note that the y-axis is presented with a square root transformation.

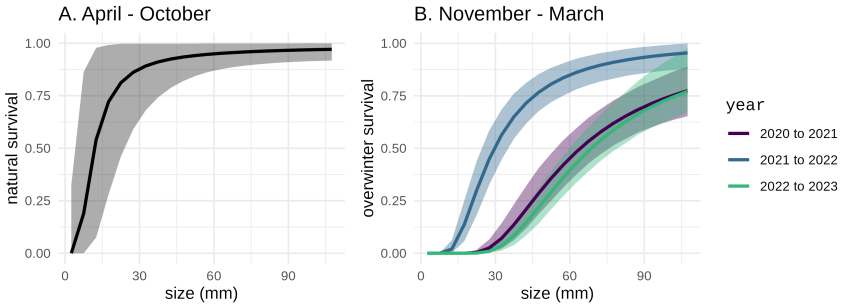

Figure 5: Size-structured natural survival rate integrated over the *A.* non-winter season between from April - October (Eq. 7) and *B.* year-specific winter season from November - March (Eq. 9). Colors indicate year, and error bars indicate the 95% credibility interval.

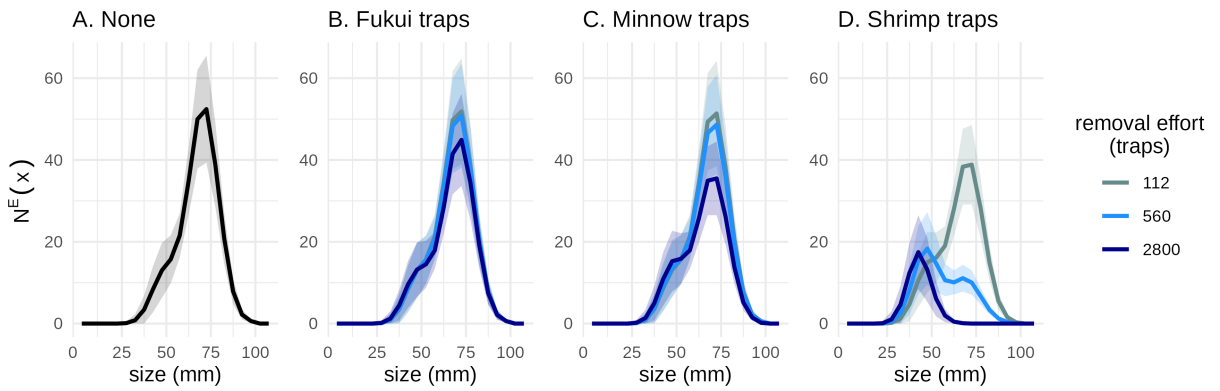

Figure 6: Population forecasts in response to varying removal efforts. Size distributions show the equilibrium crab abundance in each size class, $N^E(x)$, after overwinter mortality in April when *A.* No traps, *B.* only Fukui traps, *C.* only Minnow traps, or *D.* only Shrimp traps were applied evenly over a trapping season of 14 biweeks. Solid line indicates the median size-structured abundance across simulation replicates, and the shaded area indicates ±1 standard deviation across simulation replicates. Colors indicate total number of traps set over the trapping season.

References

Aanes, S., Engen, S., Sæther, B.-E., & Aanes, R. (2007). Estimation of the parameters of fish stock dynamics from catch-at-age data and indices of abundance: Can natural and fishing mortality be separated? *Canadian Journal of Fisheries and Aquatic Sciences*, *64*(8), 1130–1142.

Abadi, F., Gimenez, O., Arlettaz, R., & Schaub, M. (2010). An assessment of integrated population models: Bias, accuracy, and violation of the assumption of independence. *Ecology*, *91*(1), 7–14.

Abrams, P. A. (2009). When does greater mortality increase population size? the long history and diverse mechanisms underlying the hydra effect. *Ecology letters*, *12*(5), 462–474.

Aljetlawi, A. A., Sparrevik, E., & Leonardsson, K. (2004). Prey–predator size-dependent functional response: Derivation and rescaling to the real world. *Journal of Animal Ecology*, *73*(2), 239–252.

Anaya, A., Rice, D. P., & Kraft, L. J. (2025). Effect of increasing size on the ability of green crab (carcinus maenas) to manipulate and eat commercially and ecologically important species in the pacific northwest. *Fishery Bulletin*, *123*(3).

Auger-Méthé, M., Field, C., Albertsen, C. M., Derocher, A. E., Lewis, M. A., Jonsen, I. D., & Mills Flemming, J. (2016). State-space models' dirty little secrets: Even simple linear gaussian models can have estimation problems. *Scientific reports*, *6*(1), 26677.

Auger-Méthé, M., Newman, K., Cole, D., Empacher, F., Gryba, R., King, A. A., Leos-Barajas, V., Mills Flemming, J., Nielsen, A., Petris, G., et al. (2021). A guide to state–space modeling of ecological time series. *Ecological Monographs*, *91*(4), e01470.

Besbeas, P., Freeman, S. N., Morgan, B. J., & Catchpole, E. (2002). Integrating mark–recapture–recovery and census data to estimate animal abundance and demographic parameters. *Biometrics*, *58*(3), 540–547.

Beverton, R. J., & Holt, S. J. (2012). *On the dynamics of exploited fish populations* (Vol. 11). Springer Science & Business Media.

Breteler, W. K. (1976). Settlement, growth and production of the shore crab, *Carcinus maenas*, on tidal flats in the Dutch Wadden Sea. *Netherlands Journal of Sea Research*, *10*(3), 354–376.

Brockington, S., & Clarke, A. (2001). The relative influence of temperature and food on the metabolism of a marine invertebrate. *Journal of Experimental Marine Biology and Ecology*, *258*(1), 87–99.

Brooks, S. P., & Gelman, A. (1998). General methods for monitoring convergence of iterative simulations. *Journal of Computational and Graphical Statistics*, *7*(4), 434–455.

Cai, W., Santoso, A., Collins, M., Dewitte, B., Karamperidou, C., Kug, J.-S., Lengaigne, M., McPhaden, M. J., Stuecker, M. F., Taschetto, A. S., et al. (2021). Changing El Niño–Southern oscillation in a warming climate. *Nature Reviews Earth & Environment*, *2*(9), 628–644.

Carlson, S. M., Kottas, A., & Mangel, M. (2010). Bayesian analysis of size-dependent overwinter mortality from size-frequency distributions. *Ecology*, *91*(4), 1016–1024.

Carlson, S. M., Olsen, E. M., & Vøllestad, L. A. (2008). Seasonal mortality and the effect of body size: A review and an empirical test using individual data on brown trout. *Functional Ecology*, 663–673.

Claessen, D., De Roos, A. M., & Persson, L. (2004). Population dynamic theory of size–dependent cannibalism. *Proceedings of the Royal Society of London. Series B: Biological Sciences*, *271*(1537), 333–340.

Conn, P. B., Johnson, D. S., Williams, P. J., Melin, S. R., & Hooten, M. B. (2018). A guide to bayesian model checking for ecologists. *Ecological Monographs*, *88*(4), 526–542.

Contreras, H., Jaramillo, E., Duarte, C., & McLachlan, A. (2003). Population abundances, growth and natural mortality of the crustacean macroinfauna at two sand beach morphodynamic types in southern Chile. *Revista Chilena de Historia Natural*, *76*(4), 543–561.

Crall, A. W., Newman, G. J., Jarnevich, C. S., Stohlgren, T. J., Waller, D. M., & Graham, J. (2010). Improving and integrating data on invasive species collected by citizen scientists. *Biological Invasions*, *12*, 3419–3428.

Crowley, S. L., Hinchliffe, S., & McDonald, R. A. (2017). Conflict in invasive species management. *Frontiers in Ecology and the Environment*, *15*(3), 133–141.

Curtis, D., Sauchyn, L., Keddy, L., Therriault, T., & Pearce, C. (2012). *Prey preferences and relative predation rates of adult European green crabs (Carcinus maenas) on various bivalve species in British*

Columbia, Canada (tech. rep. No. 3014) (Available from Fisheries and Oceans Canada). Canadian Technical Report of Fisheries and Aquatic Sciences.

Dahlgren, J. P., & Ehrlén, J. (2011). Incorporating environmental change over succession in an integral projection model of population dynamics of a forest herb. *Oikos*, *120*(8), 1183–1190.

De Roos, A. M., Persson, L., & McCauley, E. (2003). The influence of size-dependent life-history traits on the structure and dynamics of populations and communities. *Ecology Letters*, *6*(5), 473–487.

de Valpine, P., Turek, D., Paciorek, C. J., Anderson-Bergman, C., Lang, D. T., & Bodik, R. (2017). Programming with models: Writing statistical algorithms for general model structures with nimble. *Journal of Computational and Graphical Statistics*, *26*(2), 403–413.

Dorazio, R. M., Jelks, H. L., & Jordan, F. (2005). Improving removal-based estimates of abundance by sampling a population of spatially distinct subpopulations. *Biometrics*, *61*(4), 1093–1101.

Du, J., Tepolt, C. K., Grason, E. W., McDonald, P. S., Jia, Y., & Zhang, W. G. (2024). Dispersal pathways of European green crab larvae into and throughout the eastern Salish Sea. *Progress in Oceanography*, *223*, 103245.

Duncombe, L. G. (2015). *Evaluating trapping as a method to control the european green crab, carcinus maenas, population at pipestem inlet, british columbia*. Royal Roads University (Canada).

Ellner, S. P., & Rees, M. (2006). Integral projection models for species with complex demography. *The American Naturalist*, *167*(3), 410–428.

Enberg, K., Jørgensen, C., Dunlop, E. S., Varpe, Ø., Boukal, D. S., Baulier, L., Eliassen, S., & Heino, M. (2012). Fishing-induced evolution of growth: Concepts, mechanisms and the empirical evidence. *Marine ecology*, *33*(1), 1–25.

Ergon, T., Borgan, Ø., Nater, C. R., & Vindenes, Y. (2018). The utility of mortality hazard rates in population analyses. *Methods in Ecology and Evolution*, *9*(10), 2046–2056.

Evangelista, C., Britton, R. J., & Cucherousset, J. (2015). Impacts of invasive fish removal through angling on population characteristics and juvenile growth rate. *Ecology and Evolution*, *5*(11), 2193–2202.

Fisher, M. C., Grason, E. W., Stote, A., Kelly, R. P., Litle, K., & McDonald, P. S. (2024). Invasive european green crab (carcinus maenas) predation in a washington state estuary revealed with dna metabarcoding. *Plos one*, *19*(5), e0302518.

Garbary, D. J., Miller, A. G., Williams, J., & Seymour, N. R. (2014). Drastic decline of an extensive eelgrass bed in Nova Scotia due to the activity of the invasive green crab (*Carcinus maenas*). *Marine biology*, *161*, 3–15.

García-Berthou, E., Carmona-Catot, G., Merciai, R., & Ogle, D. H. (2012). A technical note on seasonal growth models. *Reviews in Fish Biology and Fisheries*, *22*, 635–640.

Green, S. J., & Grosholz, E. D. (2021). Functional eradication as a framework for invasive species control. *Frontiers in Ecology and the Environment*, *19*(2), 98–107.

Grosholz, E. D. (2005). Recent biological invasion may hasten invasional meltdown by accelerating historical introductions. *Proceedings of the National Academy of Sciences*, *102*(4), 1088–1091.

Grosholz, E. D., Ashton, G., Bradley, M., Brown, C., Ceballos-Osuna, L., Chang, A., de Rivera, C., Gonzalez, J., Heineke, M., Marraffini, M., et al. (2021). Stage-specific overcompensation, the hydra effect, and the failure to eradicate an invasive predator. *Proceedings of the National Academy of Sciences*, *118*(12), e2003955118.

Grosholz, E. D., Lovell, S., Besedin, E., & Katz, M. (2011). Modeling the impacts of the european green crab on commercial shellfisheries. *Ecological Applications*, *21*(3), 915–924.

Grosholz, E. D., Ruiz, G. M., Dean, C. A., Shirley, K. A., Maron, J. L., & Connors, P. G. (2000). The impacts of a nonindigenous marine predator in a california bay. *Ecology*, *81*(5), 1206–1224.

Harley, S. J., Myers, R. A., & Dunn, A. (2001). Is catch-per-unit-effort proportional to abundance? *Canadian Journal of Fisheries and Aquatic Sciences*, *58*(9), 1760–1772.

Henderson, P., Holmes, R., & Bamber, R. N. (1988). Size-selective overwintering mortality in the sand smelt, Atherina boyeri risso, and its role in population regulation. *Journal of fish biology*, *33*(2), 221–233.

Hixon, M. A., Johnson, D. W., & Sogard, S. M. (2014). Boffffs: On the importance of conserving old-growth age structure in fishery populations. *ICES Journal of Marine Science*, *71*(8), 2171–2185.

Howard, B. R., Francis, F. T., Côté, I. M., & Therriault, T. W. (2019). Habitat alteration by invasive European green crab (*Carcinus maenas*) causes eelgrass loss in British Columbia, Canada. *Biological Invasions*, *21*(12), 3607–3618.

Hurst, T. (2007). Causes and consequences of winter mortality in fishes. *Journal of Fish Biology*, *71*(2), 315–345.

Jensen, G. C., McDonald, P. S., & Armstrong, D. A. (2007). Biotic resistance to green crab, Carcinus maenas, in California bays. *Marine Biology*, *151*, 2231–2243.

Jørgensen, C., Ernande, B., & Fiksen, Ø. (2009). Size-selective fishing gear and life history evolution in the northeast arctic cod. *Evolutionary Applications*, *2*(3), 356–370.

Kanary, L., Musgrave, J., Tyson, R. C., Locke, A., & Lutscher, F. (2014). Modelling the dynamics of invasion and control of competing green crab genotypes. *Theoretical Ecology*, *7*, 391–406.

Katsanevakis, S., Weber, A., Pipitone, C., Leopold, M., Cronin, M., Scheidat, M., Doyle, T. K., Buhl-Mortensen, L., Buhl-Mortensen, P., Anna, G., et al. (2012). Monitoring marine populations and communities: Methods dealing with imperfect detectability. *Aquatic Biology*, *16*(1), 31–52.

Keller, A. G., Counihan, T. D., Grosholz, E. D., & Boettiger, C. (2025). The transition from resistance to acceptance: Managing a marine invasive species in a changing world. *Journal of Applied Ecology*.

Kéry, M., & Royle, J. (2015). Modeling abundance using multinomial N-mixture models. *Applied hierarchical modeling in ecology, Kéry M, Royle JA, editors. Academic Press, Boston, Massachusetts*, 313–392.

Klassen, G. J., & Locke, A. (2007). *A biological synopsis of the European green crab, Carcinus maenas*. Citeseer.

Lapeyrolerie, M., Chapman, M. S., Norman, K. E., & Boettiger, C. (2022). Deep reinforcement learning for conservation decisions. *Methods in Ecology and Evolution*, *13*(11), 2649–2662.

Lewy, P., & Nielsen, A. (2003). Modelling stochastic fish stock dynamics using Markov Chain Monte Carlo. *ICES Journal of Marine Science*, *60*(4), 743–752.

Lowe, S., Browne, M., Boudjelas, S., De Poorter, M., et al. (2000). *100 of the world's worst invasive alien species: A selection from the global invasive species database* (Vol. 12). Invasive Species Specialist Group Auckland.

Marescot, L., Chapron, G., Chadès, I., Fackler, P. L., Duchamp, C., Marboutin, E., & Gimenez, O. (2013). Complex decisions made simple: A primer on stochastic dynamic programming. *Methods in Ecology and Evolution*, *4*(9), 872–884.

Maszczyk, P., & Brzezinski, T. (2018). Body size, maturation size, and growth rate of crustaceans. *The Natural History of the Crustacea*, *5*, 35–65.

McDonald, P. S., Jensen, G. C., & Armstrong, D. A. (2001). The competitive and predatory impacts of the nonindigenous crab *Carcinus maenas* (l.) on early benthic phase Dungeness crab *Cancer magister Dana*. *Journal of Experimental Marine Biology and Ecology*, *258*(1), 39–54.

Merow, C., Dahlgren, J. P., Metcalf, C. J. E., Childs, D. Z., Evans, M. E., Jongejans, E., Record, S., Rees, M., Salguero-Gómez, R., & McMahon, S. M. (2014). Advancing population ecology with integral projection models: A practical guide. *Methods in Ecology and Evolution*, *5*(2), 99–110.

Nicol, S., Fuller, R. A., Iwamura, T., & Chades, I. (2015). Adapting environmental management to uncertain but inevitable change. *Proceedings of the Royal Society B: Biological Sciences*, *282*(1808), 20142984.

Plard, F., Turek, D., Grüebler, M. U., & Schaub, M. (2019). IPM^2: Toward better understanding and forecasting of population dynamics. *Ecological Monographs*, *89*(3), e01364.

Prior, K. M., Adams, D. C., Klepzig, K. D., & Hulcr, J. (2018). When does invasive species removal lead to ecological recovery? implications for management success. *Biological Invasions*, *20*, 267–283.

R Core Team. (2024). *R: A language and environment for statistical computing*. R Foundation for Statistical Computing. Vienna, Austria. https://www.R-project.org/

Rees, M., Childs, D. Z., & Ellner, S. P. (2014). Building integral projection models: A user's guide. *Journal of Animal Ecology*, *83*(3), 528–545.

Riecke, T. V., Williams, P. J., Behnke, T. L., Gibson, D., Leach, A. G., Sedinger, B. S., Street, P. A., & Sedinger, J. S. (2019). Integrated population models: Model assumptions and inference. *Methods in Ecology and Evolution*, *10*(7), 1072–1082.

Rogosch, J. S., & Olden, J. D. (2021). Comparing opportunistic and strategic removal efforts to manage invasive fish species using a dynamic multi-state occupancy model. *Journal of Applied Ecology*, *58*(12), 2797–2809.

Romano, N., & Zeng, C. (2017). Cannibalism of decapod crustaceans and implications for their aquaculture: A review of its prevalence, influencing factors, and mitigating methods. *Reviews in Fisheries Science & Aquaculture*, *25*(1), 42–69.

Schnute, J., & Fournier, D. (1980). A new approach to length–frequency analysis: Growth structure. *Canadian Journal of Fisheries and Aquatic Sciences*, *37*(9), 1337–1351.

Sibert, J. R., Musyl, M. K., & Brill, R. W. (2003). Horizontal movements of bigeye tuna (*Thunnus obesus*) near Hawaii determined by Kalman filter analysis of archival tagging data. *Fisheries Oceanography*, *12*(3), 141–151.

Sogard, S. M. (1997). Size-selective mortality in the juvenile stage of teleost fishes: A review. *Bulletin of marine science*, *60*(3), 1129–1157.

Somers, I., et al. (1988). On a seasonally oscillating growth function. *Fishbyte*, *6*(1), 8–11.

Tepolt, C., Darling, J., Bagley, M., Geller, J., Blum, M., & Grosholz, E. (2009). European green crabs (*Carcinus maenas*) in the northeastern Pacific: Genetic evidence for high population connectivity and current-mediated expansion from a single introduced source population. *Diversity and Distributions*, *15*(6), 997–1009.

Tepolt, C., Grosholz, E. D., de Rivera, C. E., & Ruiz, G. M. (2022). Balanced polymorphism fuels rapid selection in an invasive crab despite high gene flow and low genetic diversity. *Molecular Ecology*, *31*(1), 55–69.

Tepolt, C., & Palumbi, S. R. (2020). Rapid adaptation to temperature via a potential genomic island of divergence in the invasive green crab, *Carcinus maenas*. *Frontiers in Ecology and Evolution*, *8*, 580701.

Thiel, M., & Dernedde, T. (1994). Recruitment of shore crabs *Carcinus maenas* on tidal flats: Mussel clumps as an important refuge for juveniles. *Helgoländer Meeresuntersuchungen*, *48*, 321–332.

Thorson, J. T., Johnson, K. F., Methot, R. D., & Taylor, I. G. (2017). Model-based estimates of effective sample size in stock assessment models using the dirichlet-multinomial distribution. *Fisheries Research*, *192*, 84–93.

Tiberti, R., Buchaca, T., Boiano, D., Knapp, R. A., Pou Rovira, Q., Tavecchia, G., Ventura, M., & Tenan, S. (2021). Alien fish eradication from high mountain lakes by multiple removal methods: Estimating residual abundance and eradication probability in open populations. *Journal of Applied Ecology*, *58*(5), 1055–1068.

Tu, C.-Y., Chen, K.-T., & Hsieh, C.-h. (2018). Fishing and temperature effects on the size structure of exploited fish stocks. *Scientific reports*, *8*(1), 7132.

Tummon Flynn, P., Poirier, L. A., Beaulieu, G., Barrett, T. J., Cairns, D. K., & Quijón, P. A. (2024). On the rebound: Removal programs yield local-scale benefits but do not sustainably suppress populations of invasive European green crabs (*Carcinus maenas*). *Biological Invasions*, *26*(2), 451–469.

Udell, B., Martin, J., Waddle, H., Johnson, F., Falk, B., Yackel Adams, A., Funck, S., Ketterlin, J., Suarez, E., Mazzotti, F., et al. (2022). Open removal models with temporary emigration and population dynamics to inform invasive animal management. *Ecology and Evolution*, *12*(8), e9173.

Walters, C. J., & Martell, S. J. (2004). *Fisheries ecology and management*. Princeton University Press.

Werner, E. E. (1994). Ontogenetic scaling of competitive relations: Size-dependent effects and responses in two anuran larvae. *Ecology*, *75*(1), 197–213.

White, J. W., Nickols, K. J., Malone, D., Carr, M. H., Starr, R. M., Cordoleani, F., Baskett, M. L., Hastings, A., & Botsford, L. W. (2016). Fitting state-space integral projection models to size-structured time series data to estimate unknown parameters. *Ecological Applications*, *26*(8), 2677–2694.

Williams, P., MacSween, C., & Rossong, M. (2009). Competition between invasive green crab (*Carcinus maenas*) and American lobster (*Homarus americanus*). *New Zealand Journal of Marine and Freshwater Research*, *43*(1), 29–33.

Yamada, S. B. (2001). *Global invader: The european green crab*. Oregon State University.

Yamada, S. B., Dumbauld, B. R., Kalin, A., Hunt, C. E., Figlar-Barnes, R., & Randall, A. (2005). Growth and persistence of a recent invader *Carcinus maenas* in estuaries of the northeastern Pacific. *Biological Invasions*, *7*, 309–321.

Yamada, S. B., Gillespie, G. E., Thomson, R. E., & Norgard, T. C. (2021). Ocean indicators predict range expansion of an introduced species: Invasion history of the European green crab *Carcinus maenas* on the North American Pacific coast. *Journal of Shellfish Research*, *40*(2), 399–413.

Young, A. M., & Elliott, J. A. (2019). Life history and population dynamics of green crabs (*Carcinus maenas*). *Fishes*, *5*(1), 4.

823 Závorka, L., Lassus, R., Britton, J. R., & Cucherousset, J. (2020). Phenotypic responses of invasive species
824 to removals affect ecosystem functioning and restoration. *Global Change Biology*, *26*(10), 5693–5704.